Chinese Chemical Letters 32 (2021) 2985–2993

Contents lists available at ScienceDirect

Chinese Chemical Letters

journal homepage: www.elsevier.com/locate/cclet

Review

A recent progress of room–temperature airborne ozone decomposition catalysts

Jiami Ma[a,1], Ranran Cao[b,1], Yanliu Dang[c], Jinlong Wang[a,*]

[a] School of Resources and Environmental Engineering, Wuhan University of Technology, Wuhan 430070, China
[b] School of Environment, Tsinghua University, Beijing 100084, China
[c] Institute of Material Science, University of Connecticut, Storrs 06269, United States

ARTICLE INFO

Article history:
Received 17 December 2020
Received in revised form 26 January 2021
Accepted 12 March 2021
Available online 15 March 2021

Keywords:
Ozone
Active sites
Mechanism
Deactivation
Indoor air
Catalysts

ABSTRACT

Ozone (O_3) plays essential roles in stratosphere and helps reduce the amount of harmful ultraviolet arriving the Earth's surface. However, O_3 is also a strong oxidant and causes troubles to human health in troposphere, especially in the confined space, such as indoor environment. Recently, O_3 abatement materials have become research hotspots due to the urgent environmental demands. Catalysis is a facile strategy that can eliminate indoor airborne O_3 efficiently and economically. Thus, this review summarizes the recent progresses of O_3 decomposition catalysts. The catalysts covered here are categorized as follows: zeolite, metal organic frameworks (MOFs), metal oxides, noble metals. Manganese–based catalysts display higher efficiency and are mainly discussed. Generally, the active sites of O_3 decomposition catalysts are described as Lewis acid sites (*e.g.*, zeolite), metal sites (*e.g.*, MOFs), oxygen vacancy sites (*e.g.*, MnO_2) in the previous work. In this review, we ascribe all the active sites to unsaturated metal sites and their Lewis acidity. Possible evidence from the experimental and theoretical perspectives are proposed. Furthermore, the strategy to circumvent deactivation caused by peroxides (O_2^{2-}) accumulation and water molecular competition are also elaborated. Finally, perspective is presented on the challenges and opportunities of exploring existing and new O_3 decomposition catalysts.
© 2021 Chinese Chemical Society and Institute of Materia Medica, Chinese Academy of Medical Sciences. Published by Elsevier B.V. All rights reserved.

1. Introduction

Ozone (O_3) is a highly reactive gas consisting of three oxygen atoms. It is both a natural product and a man–made product, and it occurs in the upper atmosphere (stratosphere) and lower atmosphere (troposphere) of the earth. Depending on where it is in the atmosphere, O_3 can affect life on Earth in good or bad ways [1,2]. Stratospheric O_3 (approximately 15–30 km above the earth surface) is formed naturally through the interaction of solar ultraviolet (UV) radiation ($\lambda < 210$ nm) with molecular oxygen (O_2) [3]. The main absorption band of O_3 is in the range of 200–300 nm with a maximum wavelength of 254 nm. It reduces the amount of harmful UV radiation reaching the Earth's surface through absorbing most UVB (280–320 nm) and the remaining part of UVC (200–280 nm) that are not blocked by ordinary oxygen in the air [4]. Tropospheric O_3 is mainly formed by photochemical reactions between two major types of air pollutants: volatile organic compounds (VOCs) and nitrogen oxides (NO_x). These reactions are considered to depend on the presence of heat and sunlight, which lead to higher ambient O_3 concentrations during the summer months [5]. For example, an hourly mixing ratio of up to 286 ppb was observed in summer 2005 at a rural mountain site north of Beijing [6]. Long–term exposure to elevated concentrations of tropospheric O_3 will cause adverse health effects, including exacerbation of breathing, pulmonary dysfunction, and hospitalization of respiratory diseases [7].

Since people spend almost 90% of their time indoors, the attention to indoor O_3 pollution should be reinforced immediately [8]. On one hand, outdoor O_3 can enter room directly through ventilation. Indoor–outdoor ratios for O_3 depend on both the air exchange rate and the rate at which O_3 is removed by indoor surfaces [9]. For example, at 2 air changes per hour, indoor O_3 levels are typically 35% of outdoor levels. It exceeds 50 parts per billion (ppb) in places with severe photochemical smog [10]. On the other hand, O_3 is also generated by corona discharge. Rooms with printers or electrostatic ventilation system usually emit excess O_3. Valuntaite and Girgzdiene [11] reported that the average O_3 concentration near the copy machine was 280 ± 63 μg/m^3. Moreover, in some specifically confined space, such as cabins

* Corresponding author.
E-mail address: wjl16@whut.edu.cn (J. Wang).
[1] These authors contribute equally to this work.

https://doi.org/10.1016/j.cclet.2021.03.031
1001-8417/© 2021 Chinese Chemical Society and Institute of Materia Medica, Chinese Academy of Medical Sciences. Published by Elsevier B.V. All rights reserved.

[12], hospitals [13] or water treatment plants [14], the concertation of O_3 obviously exceeds standard limits (Chinese indoor quality standard, GB/T 18883–2020, below 0.08 ppm, average per 1 h). In addition to the endanger of O_3, indoor O_3 also reacts rapidly with some organics, especially those containing unsaturated carbon–carbon bonds, which increase the risk of exposure to more toxic pollutants. For example, the concentration formaldehyde, acetaldehyde, and aldehydes involving 5–10 carbons dramatically increase at the presence of O_3 [10]. Thus, it is vitally important to study the methods and materials for indoor O_3 elimination [15,16].

Various methods have been attempted to control O_3 emission, including physical and chemical adsorption, thermal decomposition, and catalytic decomposition. For example, the modified activated carbon (AC; HNO_3 treatment) in Subrahmanyam's work shows the stable O_3 conversion as long as 12 h on stream [17]. However, the stability of AC is not long-lasting, since surface carbon will be easily oxidized at the initial stage and the O_3 removal efficiency drops dramatically after that. In addition, liquid sodium carbonate or potassium iodide works well for O_3 removal [18]. With higher KI loadings (1.2 g), denuders can be used at 20 L/min to remove O_3 for several days in the Los Angeles atmosphere under conditions of mild to severe photochemical smog [19]. However, pH condition of the solution needs to be seriously controlled [18], which increases the barrier for its real application. Furthermore, O_3 can also be thermally decomposed within 1.5 s at the temperature of 250 °C [2]. The high energy consumption and the serious influence of indoor comfort make this technique inapplicable. UV–assisted photocatlysis is another strategy that can eliminate indoor O_3 [20,21]. In addition, it is also effective for indoor bio-aerosols disinfection [22]. However, this technique needs relatively long residence time (seconds level). Considering indoor ventilation efficiency, the O_3 removal catalysts used in the ventilation system need to be workable at a very short residence time (a few hundredths of a second). Room–temperature catalysis using metals or metal oxides (*e.g.*, MnO_2, NiO, Pd, Ag) seems to be more attractive for the removal of O_3 due to its advantages of mild reaction conditions, high efficiency and low energy consumption.

In this review, we put more emphasis on the room–temperature airborne O_3 decomposition catalysts, which includes zeolite, metal organic frameworks (MOFs), metal oxides, and noble metals. The active sites and deactivation mechanism are also elaborated. We hope this review will be helpful to guild the modification of current catalysts and highlight prospect in developing new catalysts regarding the long–term O_3 elimination, especially in the real environment.

2. Room-temperature catalysis

Catalysis includes homogeneous and heterogeneous reaction. Homogeneous O_3 decomposition mostly occurs in stratosphere with free radicals, such as hydroxyl radical ($^{\bullet}OH$), nitric oxide radical ($NO^{\bullet}$), chlorine radical ($Cl^{\bullet}$) and bromine radical ($Br^{\bullet}$) [23,24]. This part will not be discussed here because the purpose of this review focuses on the control of indoor O_3. Heterogeneous O_3 catalysis, especially room–temperature catalysts, can be used in the ventilation system or used as indoor cleaner to reduce indoor O_3 concentration. Since the 1970s, scholars in various countries have carried out the research of O_3 decomposition with heterogeneous catalysts. Li *et al.* [25,26] studied the O_3 decomposition mechanism over MnO_2/γ–Al_2O_3 catalyst by *in–situ* Raman and ^{18}O isotope substitution experiment. The O_3 decomposition mechanism under dry condition can be simply described as follows (Fig. 1a): First, O_3 undergoes dissociative adsorption on the surface to form an oxygen molecule and an atomic oxygen; Then, the atomic oxygen further reacts with the gaseous O_3 molecule to form an adsorbed O_2^{2-} and gaseous oxygen molecules; Finally, the O_2^{2-} intermediate is decomposed to form oxygen molecules and desorbed from the catalyst surface. However, when the relative humidity is high, the entire mechanism seems to be completely changed (Fig. 1b). Water first dissociates at active site to form surface OH. Then, O_3 might react with surface OH with the release of $HO_3^{\bullet}$. Then $HO_3^{\bullet}$ will be transformed into $^{\bullet}OH$ and $^{\bullet}OOH$. Finally, another O_3 will react with $^{\bullet}OOH$ with the generation of H_2O and O_2. The former mechanism is widely accepted while the latter one is still doubtable and needs further evidence.

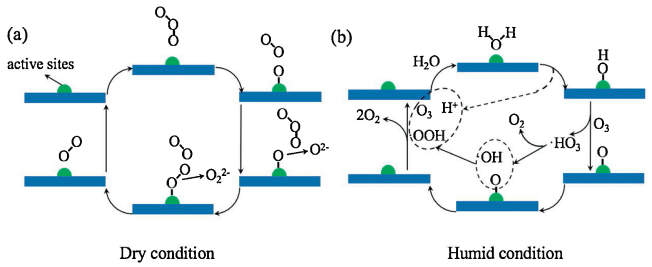

Fig. 1. O_3 decomposition mechanism under (a) dry and (b) humid condition.

Up to now, the active components of the solid catalysts include zeolite, metal organic frameworks (MOFs), metal oxides, noble metals and so on. Most of the reported catalysts can decompose O_3 at ambient temperature and exhibit good stability [1,2,15,16]. The category and advantages/disadvantages of different types of catalysts are shown in Table 1. Details of the catalysts will be discussed in the following part.

3. Ozone decomposition catalysts

3.1. Zeolite

Zeolite with microporous structure can work at room temperature for O_3 decomposition. More and more researches ascribe the active site of zeolite to Lewis acid sites, because O_3 could act like a Lewis base according to its resonance structure [27]. Lewis acidity in a zeolite generally results from isolated aluminum, which can accept electron pairs due to its uncoordinated structure [28]. As a result, the content of Lewis acid sites in a tetrahedral zeolite framework can be adjusted by using aluminum (Al) substitutes for silicon (Si). Brodu *et al.* [29] synthesized ZSM–5 zeolites with three ratios of Si/Al (78, 360, 2100). ZSM–5 with lowest Si/Al ratio, *i.e.*, highest acid site, exhibits the best performance for O_3 decomposition. The strength of acid site was also investigated. ZSM–5 with lowest Si/Al ratio features 17% strong acid site, which is favorable for O_3 decomposition. The strong Lewis acid sites favor the decomposition of O_3, whereas the weak acid sites adsorb O_3 molecular. In addition, ammonium ion–exchange treatment follows thermal treatment can also adjust the density and strength of Lewis acid sites [30]. Furthermore, the pore size is also very important for the diffusion of O_3 to the active site in Zeolite. Brodu *et al.* [31] studied the effect of zeolite framework and pore width on the efficiency of decomposition of gaseous O_3. Compared with microporous zeolite (H–FAU) and interconnected channels zeolite (H–MFI, Na–MFI), parallel channels H–MOR displays the highest efficiency for O_3 decomposition. It shows channels or cages with slightly larger size than that of O_3 molecules promote the interaction between O_3 and Lewis acid sites. Although lots of modifications have been made on zeolite, the O_3 decomposition activity of zeolite is still limited due to the intimate occupation of strong Lewis acid sites by peroxide and atomic oxygen.

Table 1
The category and advantages/disadvantages of different types of room-temperature O_3 decomposition catalysts.

Lists	Specifics	Advantages	Disadvantages
Zeolite	NH4Z3, ZSM-5-87, H-MOR	Structure stability	Low efficiency
MOFs	MIL-100	Water promoted effect	Weak structure stability
Metal oxides	Pristine MnO_2, Modified MnO_2, Cu_2O, ZnO, $LaFeO_3$, Fe_2O_3, NiO, *etc.*	High efficiency at dry condition; cost-effective	Deactivation at high RH
Nobel metals	Pd, Pt, Au, Ag or Ag_2O *etc.*	High efficiency at dry and humid condition	High costs

3.2. MOFs

Metal–organic frameworks (MOFs) are a class of compounds consisting of metal ions or clusters that coordinate with organic ligands to form one–, two–, or three–dimensional structures [32]. Wang *et al.* [33] proposed an iron–containing metal organic framework, MIL–100(Fe), for O_3 removal. In Fig. 2, the results show that MIL–100(Fe) exhibits 100% persistent O_3 conversion efficiency in 100 h at 45% relative humidity and space velocity of $1.9 \times 10^5\ h^{-1}$ at room temperature. The high efficiency and long–term O_3 decomposition activity are ascribed to its porous structure and highly dispersed Fe^{3+} active sites. More interestingly, presence of water is favorable for O_3 elimination, and decomposition rate of O_3 is enhanced and with relative humidity ranging from 40% to more than 90%. The O_3 decomposition activity over zeolites and MOFs are displayed in Table 2.

3.3. Metal oxides

Metal oxides–type of O_3 catalysts have been rapidly developed during the last 5 years. Heisig *et al.* [34] found the the order of catalytic activity of different materials followed: $MnO_2 > Co_3O_4 > NiO > Fe_2O_3 > Ag_2O > Cr_2O_3 > CeO_2 > MgO > V_2O_5 > CuO > MoO_3$, when experiments were carried out at a temperature of 313 K, O_3 concentration of 2 ppm, relative humidity of 40%, and flow rate of 1.8 L/s. In this part, manganese oxides especially MnO_2, presenting outstanding O_3 decomposition activity are mainly discussed among all kinds of metal oxides.

3.3.1. Manganese oxides

Jia *et al.* [35,36] found that the crystal structure and morphology of manganese dioxide (MnO_2) have a significant impact on its catalytic activity for the decomposition of O_3. Among them, the activity of α–MnO_2 is better than that of β–MnO_2 and γ–MnO_2, and the activity of nanofiber α–MnO_2 is higher than that of nanorod and tubular α–MnO_2. Oxygen vacancy (V_O) is the decisive factor of catalytic activity. The content and the disperse of V_O in MnO_2 affect the catalytic activity of O_3 decomposition. The function of V_O is shown in Fig. 3. Through the *in–situ* Raman observation, the decomposition of the peroxide species (O_2^{2-}) on the catalyst surface is the rate–limiting step. Liu *et al.* [37] also ascribed the higher activity of amorphous MnO_x to its abundant V_O. In addition, larger specific surface area and mixed Mn^{2+}, Mn^{3+} and Mn^{4+} in the amorphous mesoporous MnO_x also facilitate the O_3 decomposition rate.

Since V_O in MnO_2 is the decisive factor for O_3 decomposition, more and more work focus on the generation of V_O on MnO_2. Zhu *et al.* [38] obtained α–MnO_2 nanofibers with high surface V_O by vacuum deoxidation method. The formation of surface V_O greatly improves the adsorption and decomposition of O_3 molecules on the surface of α–MnO_2. After that, Zhu *et al.* [39] treated α–MnO_2 nanowires with adjustable K^+ concentration through hydrothermal process in KOH solution. The results indicate that the catalyst life increases from 3 h to 15 h comparing with the untreated sample. This is mainly due to the electrostatic interaction between the oxygen atom in the tunnel and the introduced K^+, which results in a large number of active V_O, thus improving the performance of the catalyst. Similar phenomena are also observed on Na^+ doped OMS–2 sample [40]. The introduction of Na^+ in the tunnel framework of OMS–2 facilitates lattice defect formation. In addition, the substitution of K^+ by larger or smaller ions such as protons and Ag^+ can also result in more V_O [41,42]. For example, Ag^+ can be well dispersed in the microtunnels of α–MnO_2 without destroying the original tunnel structure. The nonstoichiometric changes in the local structure increase the presences of V_O [42]. Furthermore, element doping is a traditional and effective strategy that can optimize electronic and geometric and structures of catalytic centers [43]. Jia *et al.* [44] prepared iron–modified manganese oxide (Fe–MnO_x), and found the obtained Fe–MnO_x catalyst contained more V_O, which made O_3 decomposition rate high in dry/humid air. Li *et al.* [45] synthesized the metal (cerium and cobalt) doped γ–MnO_2 catalyst for O_3 decomposition. The results show that the O_3 conversion rate follows: Ce–γ–MnO_2 (96%) > Co–γ–MnO_2 (55%) > γ–MnO_2 (38%). The introduction of Ce creates more V_O, and also increases the specific surface area, which facilitates O_3 adsorption and decomposition. Ma *et al.* [46] used cryptomelane as a model and further investigated the doping mechanism. Co^{3+} and Fe^{3+} replace Mn^{3+} in the structure of cryptomelane, while Ce^{4+} mainly replaces K^+ in the tunnel and partially replaces Mn^{4+} in the structure. The former inhibits O_3 decomposition while the later facilitates, because the content of Mn^{3+} and surface V_O play key roles in O_3 decomposition. Furthermore, the introduction of tinstone (W) and vanadium (V) on α–MnO_2 also promote the O_3 decomposition activity [47,48]. MnO, Mn_2O_3 and $MnCO_3$ also display O_3 decomposition activity [49–52]. For example, Yu *et al.* [49] fabricated AC based MnO

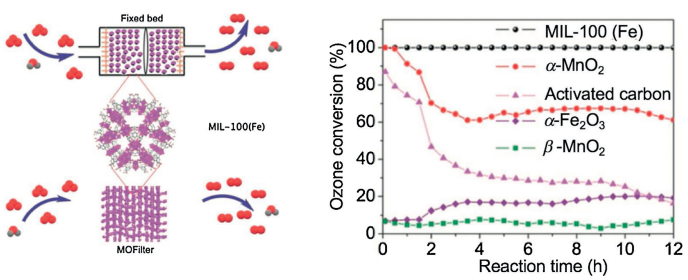

Fig. 2. The structure and O_3 decomposition activity of MIL–100(Fe). Reproduced with permission [33]. Copyright 2018, Wiley.

Table 2
The O_3 decomposition activity over zeolites and MOFs.

Catalyst	O_3 concentration (ppm)	Temperature (°C)	Relative humidity (%)	GHSV (L g_{cat}^{-1} h^{-1})	Reaction time (h)	O_3 conversion (%)	Reaction rate (μg g_{cat}^{-1} min^{-1})	Ref.
ZSM–5–78	3256	20	–	30	1	100	3250443.6	[29]
NH4Z3	8.3	20	–	296	1.7	40	32701.4	[30]
H–MOR	7513	20	–	30	2	90–100	–	[31]
MIL–100(Fe)	45	25	45	2000	12	100	2944.6	[33]

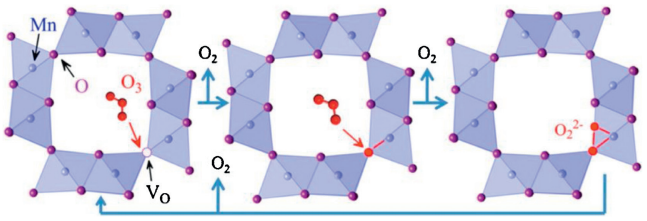

Fig. 3. Illustration of V_O in O_3 decomposition process. Reproduced with permission [35]. Copyright 2016, Elsevier.

catalyst. The minimum size of MnO nanoparticles and the maximum surface V_O synthesized at 700 °C of calcination are responsible for the enhanced O_3 decomposition rate. Ma *et al.* [50] found α–Mn_2O_3 can also decompose O_3, and it activity can be increased by a factor of 2.5 with the addition of Ce. The O_3 decomposition activity over manganese-based catalysts are shown in Table 3 [35–40,44–51,53–68].

3.3.2. Other metal oxides

Mathew *et al.* [69] prepared a mesoporous two–line ferrihydrite (M2LFh), whereas unsaturated FeO_x species are widely existed on the surface. M_2LFh exhibits about 43.5 times higher O_3 removal rate than commercial Fe_2O_3 at room temperature. The tricoordinated Fe site can result in more deformation of O_3 molecular comparing with tracoordinated one (O(I)–O(II) distance: 1.52 *vs.* 1.37 Å), which facilitates O_3 decomposition. Gong *et al.* [70] prepared Cu_2O nanoparticles with different exposed facets, *i.e.*, (100) and (111) (Fig. 4). Cu_2O with (100) plane has the higher O_3 conversion efficiency comparing with (111) facet, because O_2^{2-} adsorbs onto the (100) plane by two shared bonds, which is weaker

Table 3
The O_3 decomposition activity over manganese-based catalysts.

Catalyst	O_3 concentration (ppm)	Temperature (°C)	Relative humidity (%)	GHSV (L g_{cat}^{-1} h^{-1})	Reaction time (h)	O_3 conversion (%)	Reaction rate (μg g_{cat}^{-1} min^{-1})	Ref.
α–MnO_2	14	5	1	660	2	100	324.0	[35]
γ–MnO_2	14	60	1	660	2	100	270.5	
β–MnO_2	14	100	1	660	2	100	241.5	
α–MnO_2 nanofibers	23	25	45	880	1.5	80	529.7	[36]
α–MnO_2 nanorods	23	25	45	880	1.5	60	397.3	
α–MnO_2 nanotubes	23	25	45	880	1.5	50	331.1	
MnO_x–I	20	25	50	600	12	100	392.6	[37]
Vac–200–4h	20	25	< 5	540	12	97	342.7	[38]
KOH–4h	50	25	30	540	15	78	689.0	[39]
$NaMn_3$	45	25	60	660	6	70	680.2	[40]
Fe–α–MnO_x	100	25	60	660	6	73	1576.3	[44]
γ–MnO_2	40	30	65	840	6	38	410.8	[45]
Ce–γ–MnO_2	40	30	65	840	6	96	1037.9	
Co–γ–MnO_2	40	30	65	840	6	55	594.6	
OMS–2	40	30	45	600	6	100	772.2	[46]
Ce–OMS–2	40	30	45	600	6	100	772.2	
Co–OMS–2	40	30	45	600	6	65	501.9	
Fe–OMS–2	40	30	45	600	6	50	386.1	
W–α–MnO_2	120	25	65	660	4	50	1295.6	[47]
V–α–MnO_2	110	25	55	600	5	50	1079.7	[48]
MnO/AC–700	30	25	45	1200	10	85.9	1011.7	[49]
α–Mn_2O_3	40	30	65	840	6	40	432.4	[50]
$CeMn_{10}O_x$	40	30	65	840	6	40	1104.0	
$MnCO_3$	14	25	–	460	22	85	179.1	[51]
Ce-γ-MnO_2 (pH 7)	40	30	65	300	6	98	420	[53]
α–MnO_2 sheets	60	–10	–	460	–	100	1023.1	[54]
H–MnO_2 (acid)	115	25	50	600	5	60	1354.5	[55]
50–1–N–MnO_2	115	25	50	600	6	80	1806.0	[56]
Ce–MnO_2(300)	115	25	–	1200	5	98	4424.8	[57]
Ce–MnO_2(0.28)	55	25	–	1200	3	98	2116.2	[58]
MnO_2–300	20	25	50	600	12	100	392.6	[59]
S–300	120	25	50	600	6	65	1531.2	[60]
$MnFe_{0.5}O_x$	10000	25	90	12	8	90	3533.5	[61]
OMS–2–Ac	40	30	45	600	6	100	772.2	[62]
Co–MnO_x(0.36)–Al	1000	25	dry gas	48	12	100	1570.4	[63]
K–δ–MnO_2	2000	30	dry gas	600	6	35	13514.8	[64]
H–δ–MnO_2	2000	30	dry gas	600	8	100	38613.8	
Ce–OMS–2–80%	40	30	45	600	6	97	749.1	[65]
pH – 7 (Ce–γ–MnO_2)	40	30	65	300	6	96	370.6	[66]
Ce–OMS–2 (95–100 °C)	40	30	90	600	6	90	695.0	[67]
Ce-OMS-2-80%	40	30	45	600	6	97	831.4	[68]

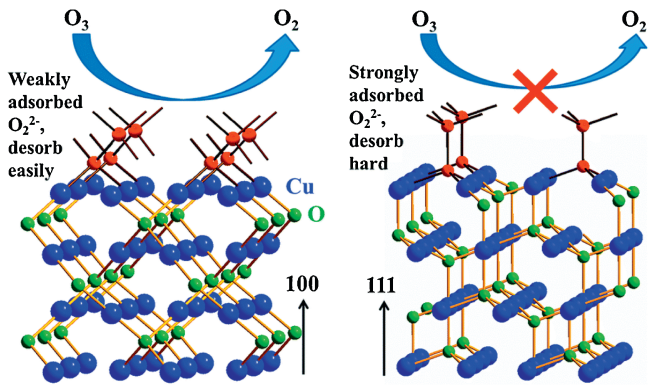

Fig. 4. Schematics of O_3 decomposition on (100) and (111) surface planes of Cu_2O. Reproduced with permission [70]. Copyright 2017, Royal Society of Chemistry.

than the three bonds on (111). NiO can also decompose O_3 effectively. However, it activity will be inhibited in the presence of water due to its strong intimation with water, resulting in the block of surface active sites. When Ni is introduced, on one hand, the electron transfer from NiO to Ni may promote the electron release of O_2^{2-}; one the other hand, lattice expansion in Ni–supported NiO caused by lattice mismatch is good for the movement of adsorbed OH, which can weaken competitive adsorption of H_2O [71]. Wang *et al.* [72] created a lot of V_O on ZnO, and revealed the relationship between catalyst activity and surface V_O. Modified ZnO by H_2 reduction and Ga/Li doping can maintain 30% O_3 degradation rate at 6 h for 20 ppm of O_3 and 240,000 mL g^{-1} h^{-1} of GHSV.

3.3.3. Supported or hybrid metal oxides

The carrier may affect the geometric and electronic structure of the surface–active components. Under the same preparation conditions, MnO_x displays monomeric type on Al_2O_3 supported sample while it shows multinuclear structure for the other supports. In addition, the support also results in different numbers of empty d–states of MnO_x, affecting the entire O_3 decomposition rate [73]. Carbon material is a commonly used support. Ji *et al.* [74] immobilized MnO_x on carbon nanotubes. The large specific surface area and enhanced ability of electron transfer from CNTs to MnO_x might be responsible for the enhanced activity towards O_3 decomposition. Similar phenomena were also reported on Graphene based Cu_2O hybrid catalyst, easy electron transfer at contacted interface promotes O_3 decomposition [75]. Besides, based on the concept of Lewis acid sites and surface V_O, O_3 tends to be nucleophilic rather than electrophilic. The promoted activity maybe the synergistic effect from both metal oxides and carbon materials.

Using bimetallic oxides for O_3 decomposition were also investigated. Heisig *et al.* [34] loaded the above–mentioned active single metal oxides and bimetallic oxides on the activated carbon, and found that the activity of bimetallic oxides was significantly higher than that of single metal oxides. The order of activity was as follows: Mn–Fe (87%) > Co–Fe (80%) > Mn−CO (78%) > Mn–Ni (74%) > Fe–Ni (71%) > Co–Ni (55%). Because of the interaction between MnO_2 and Fe_2O_3, Mn–Fe system showed the best catalytic activity for O_3 decomposition. In addition, perovskite–type mixed oxides, such as $LaFeO_3$ was also prepared and tested O_3 decomposition activity. Comparing with commercial Fe_2O_3, $LaFeO_3$ shows higher O_3 decomposition both in dry and humid conditions. It is because $LaFeO_3$ shows no structure deformation, no O_2^{2-} accumulation, high density of acid site, and easy water desorption. Moreover, the replacement of Fe atom by Ni increases the content of Fe^{2+}, promoting O_3 decomposition [76]. The O_3 decomposition activity over manganese-free metal oxides mentioned above are shown in Table 4 [69–72,75–77].

3.4. Nobel metal catalysts

Supported nobel metals are efficient catalysts for the decomposition of gaseous O_3 [1,78]. For example, Hao *et al.* [79] reported Au/Fe_2O_3 prepared by precipitation have good O_3 removal activity. When the temperature was 0 °C, the relative humidity was 5%, the initial concentration of O_3 was 3000 ppm, and the GHSV was 10,000 h^{-1}, the catalytic activity of O_3 decomposition was as high as 98% after 15 h reaction while single Fe_2O_3 dropped to 41% within 1 h. Zhang *et al.* [80] loaded Au particles on coal–based AC (Au/AC) and tested its O_3 decomposition activity in a more realistic condition. In the case of high space velocity of 120,000 h^{-1}, O_3 concentration of 50 mg/m^3, and relative humidity of 45%, the Au/AC catalyst still exhibits 90.7% O_3 removal efficiency as long as 2500 min. Promoted activity is also observed on Pd–based catalyst [81,82]. However, the high price of the noble metals restricts wide application and has been encouraged the use of less expensive catalysts. Ag catalyst especially in the state of Ag_2O, exhibits obviously better activity comparing with commercial Fe_2O_3, Co_3O_4, CeO_2, Mn_2O_3, CuO, Pb_2O_3, Bi_2O_3, SnO_2, MoO_3, V_2O_5 catalyst when

Table 4
The O_3 decomposition activity over manganese-free metal oxides.

Catalyst	O_3 concentration (ppm)	Temperature (°C)	Relative humidity (%)	GHSV (L g_{cat}^{-1} h^{-1})	Reaction time (h)	O_3 conversion (%)	Reaction rate (μg g_{cat}^{-1} min^{-1})	Ref.
M_2LFh (Mesoporous two–line Ferrihydrite)	600	Room temperature	–	1500		95	–	[69]
Cu_2O cube–40 nm	200	25	80	60	8	100	392.6	[70]
	200	0	dry gas	60	2.5	100	428.5	
	770	25	dry gas	60	6	100	1511.5	
Ni/NiO	1000	25	dry gas	240	8	100	7852.3	[71]
	1000	25	90	240	8	98	7695.3	
ZnO	20	25	–	240	6	30	46.6	[72]
Cu_2O/rGO	20	25	dry gas	60	10	100	39.2	[75]
	20	25	90	60	10	96	37.6	
$LaFeO_3$	1000	25	dry gas	240	8	100	7852.3	[76]
	1000	25	90	240	4	70	5496.6	
$LaFe_{0.95}Ni_{0.05}O_3$	1000	25	dry gas	240	8	97.7	7671.7	
	1000	25	90	240	4	93	7302.6	
Cu_2O–CuO–$Cu(OH)_2$	20	25	dry gas	240	30	100	157.0	[77]
	20	25	90	240	16	82	128.7	

the O_3 concentration is 3000 ppm; GHSV is 9000 h^{-1}; reaction time is 10 min [83]. The advantage of precious metal catalysts is that they can maintain high O_3 decomposition activity under high relative humidity conditions. Tao *et al.* [84] found Pd-Co-MnOx/Al_2O_3 catalyst exhibits high moisture tolerance. The introduction of Pd weakens H_2O adsorption on the catalyst surface. Similar phenomenon was also observed on Ag modified MnO_2 catalysts [85,86]. The O_3 decomposition activity over noble metal catalysts are shown in Table 5 [79–82,84,85,87–90]. The influence of the noble metals on the moisture resistance will be systematically discussed in Part 4.

4. Active sites clarification & deactivation mechanism

4.1. Clarification of active sites

From the above analysis, the active sites of O_3 decomposition catalysts are described as Lewis acid sites (*e.g.*, zeolite), metal sites (*e.g.*, FeO_x or MOFs) and V_O sites (*e.g.*, MnO_2) in the previous work. Here, we try to ascribe all the active sites to unsaturated metal sites. For example, the unsaturated coordination structure of Al in zeolite makes it feature extra empty orbit to accept electron pairs from O_3. Other researchers also regard unsaturated metal atom, such as Fe atom in FeO_x and Fe-MOFs, as active site and use this site to analyze O_3 adsorption energy and reaction pathways [33,46,76]. For MnO_2 catalyst, all literatures classify the O_3 active site as V_O. Considering that O_3 can interact with adjacent manganese atoms after being adsorbed at V_O, thus, we regard manganese atoms that are not saturate coordinated as active sites for O_3 decomposition. Unsaturated metal sites with different geometric and electronic states usually exhibit various catalytic properties. For example, Li *et al.* [53] proposed there are two kinds of V_O on α-MnO_2 (sp^2 hybridized V_O and sp^3 hybridized V_O), showing different characteristics for the decomposition of O_3. sp^2-V_O is more intimate to oxygen species. The adsorbed oxygen at sp^2 hybridized V_O site is difficult to be desorbed, making catalyst deactivated. Thus, it is not accurate to ascribe O_3 decomposition active site to all unsaturated metal atoms.

Considering unoccupied d orbitals in metal active sites are Lewis acid sites that can accept electron pairs from O_3, we further explain O_3 decomposition active sites from the perspective of Lewis acid-base pairs. MnO_2 catalyst with V_O (removing an O atom will leave behind two unpaired electrons) is regarded as Lewis base. The presence of Lewis base on MnO_2 will increase the binding energy with a Lewis acid site (Mn site vacated by the V_O), *i.e.*, the strength of Lewis acid will be weakened [91]. Jia *et al.* also reported that the presence of V_O resulted in the weaken of Lewis acid site, demonstrated by NH_3–TPD [35]. This phenomenon can also be explained by the increased content of Mn^{3+} due to V_O [35,38]. The strength of Lewis acid for Mn^{3+} is 1.698, while it increases to 1.874 for Mn^{4+}, further confirming the V_O's negative effect on the strength of Lewis acid [92]. Lewis acid site facilitates to O_3 adsorption and decomposition [29–31]. However, too strong Lewis acid site might suppress its activity. Suitable Lewis acid site benefits for O_3 polarization and subsequent electron transfer.

4.2. Deactivation mechanism

Deactivation is one of the biggest challenges in the use of catalyst. In the process of O_3 decomposition, deactivation mainly includes two aspects: accumulation of O_2^{2-} and inhibition by moisture.

4.2.1. Accumulation of O_2^{2-}

In the dry atmosphere, the rate–limiting step of O_3 decomposition on the catalysts is the desorption of adsorbed O_2^{2-} intermediate to produce O_2 [25,26]. This step requires the electron transfer from the adsorbed species (*i.e.*, O_2^{2-}) to the active center (*i.e.*, unsaturated metal site). For example, Chen *et al.* [54] compared two kinds of tunneled MnO_2, *i.e.*, α–MnO_2 and β–MnO_2. α–MnO_2 processes higher O_3 decomposition activity comparing with β–MnO_2. The gap of HOMO (O_2^{2-})–LUMO (Mn^{4+}) governs the electron transfer. The e_g orbitals of Mn^{4+} can accept electrons from O_2^{2-}. The α–MnO_2 features the down–shifted $2p_{3/2} \rightarrow 3d$ (e_g) transition, which reduces the energy gap between HOMO of O_2^{2-} and LUMO of Mn^{4+}, *i.e.*, benefiting for electron transfer [93]. The schematic illustration of the relative energy levels of the HOMO and LUMO, and the orbitals of the O_2^{2-} intermediate and Mn^{4+} are shown in Fig. 5.

The accumulation of O_2^{2-} can be observed through spectroscopy methodology. High contents of adsorbed O_2^{2-} and atomic oxygen species are observed ZSM–5 zeolite *via in–situ* Diffuse reflectance infrared Fourier transform spectroscopy (DRIFTS), which occupy Lewis acid site and are harmful to the catalyst [29]. In addition, obvious O_2^{2-} related species were also observed on MnO_2 catalyst *via in–situ* Raman and DRIFTS and the valance state of MnO_2 increases as the reaction proceeds, inhibiting the electron transfer from O_2^{2-} species to Mn^{3+}/Mn^{4+}. Strategies that are commonly used to overcome the accumulation of O_2^{2-} are as follows:

(a) Modification of fresh catalysts. In order to facilitate electron transfer, the reducibility of the active center needs to be modified. For example, doping MnO_2 with Fe, Ce, W, V [44–48]

Table 5
The O_3 decomposition activity over noble metal catalysts.

Catalyst	O_3 concentration (ppm)	Temperature (°C)	Relative humidity (%)	GHSV (L g_{cat}^{-1} h^{-1})	Reaction time (h)	O_3 conversion (%)	Reaction rate (μg g_{cat}^{-1} min^{-1})	Ref.
Au/NiO (1 at%)	3000	0	5	10000	15	95	–	[79]
Au/Fe_2O_3 (1 at%)	3000	0	5	10000	15	98	–	
Au/AC	25	Room temperature	45	120000	42	90.7	–	[80]
Pd–Mn/SiO_2–Al_2O_3 (PM350)	60	40	55%–65%	635,000	80	90	–	[81]
Pd-Ce-OMS-2 (0.5 at%)	40	30	90	600	720	>90	771.4	[82]
Pd-Co-MnO_x-Al (0.1 at%)	1500	25	50	48	6	100	2571.4	[84]
Co-MnO_x-Al (0.1 at%)						90	2314.2	
Ag-Co-MnO_x-Al (0.1 at%)						75	1928.6	
Pt-Co-MnO_x-Al (0.1 at%)						62	1594.3	
6%Ag/α-Mn_2O_3-I	40	30	65	840	6	99	1188	[85]
Pd-Ce-OMS-2 (3.0 at%)	40	30	90	1200	6	100	1714.3	[87]
	40	30	90	1400	6	84	1680	
Pd/Al_2O_3	0.2	30	50	176	–	78	–	[88]
Pd/MnO_2	510	26	90	15	120	90	–	[89]
Ag-H-MCM-41	4390	23	Dry	133	6	94	–	[90]

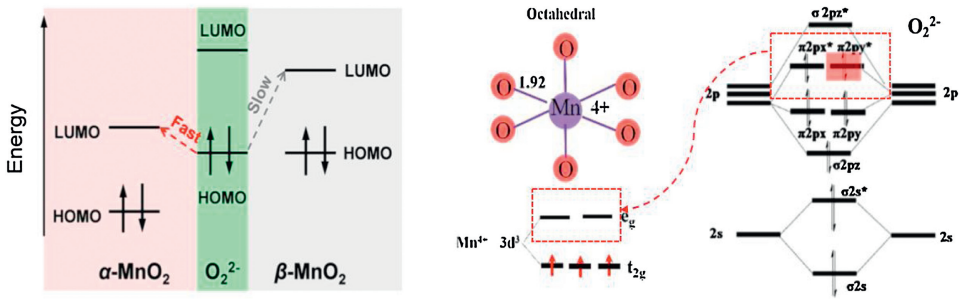

Fig. 5. Schematic illustration of electron transfer from the relative energy levels of the HOMO and LUMO of the O_2^{2-} HOMO to Mn^{4+} LUMO. Reproduced with permission [54,93]. Copyright 2018, ACS & 2018, Elsevier.

can deduce the average oxidation state in MnO_2, benefiting for the electron transfer from O_2^{2-} species to Mn^{3+}/Mn^{4+}. In addition, unstable active sites are easier to combine with O_2^{2-}, making the desorption of intermediate products more difficult. Hong *et al.* [40] found that oxygen vacancy formation energy decreased onced Na^+ was introduced in the tunnel framework of OMS-2, which can make accumulated O_2^{2-} species easily desorbed. Furthermore, composite the catalyst with a material with strong electrical conductivity can promote the electron transfer of O_2^{2-}. Ji *et al.* [74] found immobilized MnO_x on carbon nanotubes can enhance the O_2^{2-} electron transfer at contacted interface.

(b) Post-treatment of the catalysts. It is generally considered the deactivation of catalyst is accompanied by the filling out of the oxygen vacancy. High temperature treatment can partially restore catalyst activity. For example, Hong *et al.* [40] used 425 °C calcination under N_2 atmosphere to treat used Na–OMS–2 and recovered its activity. The calcination temperature can be further decreased by 75 °C in MnO_x based Ag catalyst [85].

4.2.2. Inhibition of moisture

Moisture is another important factor that affects the activity of the catalyst [55,56]. Take MnO_2 catalyst as an example, the adsorption energy of H_2O, O_2, and O_3 on the (110) surface of V_O and V_O free α–MnO_2 is shown in Fig. 6. The adsorption energies of H_2O and O_3 reduce from −0.5877 eV to −0.8746 eV, and −0.4448 to −3.3595 eV due to the formation of surface V_O. Though O_3 molecule dominates the adsorption process, the competitive

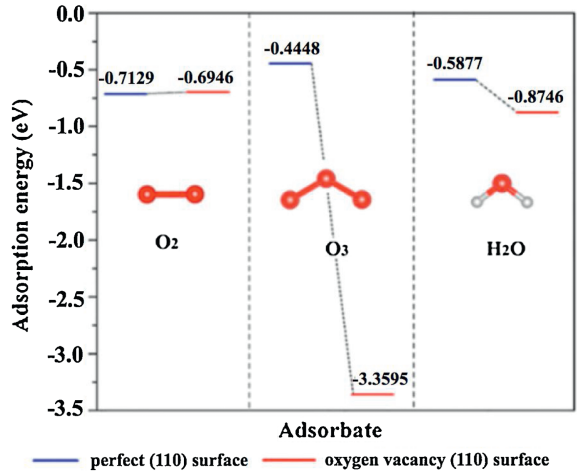

Fig. 6. The adsorption energy of H_2O, O_2, and O_3 on the (110) surface of V_O and V_O free α–MnO_2. Reproduced with permission [38]. Copyright 2017, Elsevier.

adsorption of H_2O molecule over V_O site cannot be ignored [38]. In addition, under high moisture, the process of gas phase ozone decomposition is similar to that of catalytic ozonation in water because water will be condensed on the surface of catalyst, especially under high relative humidity [94].

A free radical–based O_3 decomposition mechanism might also exist. O_3 can react with surface OH with the generation of $HO_3^{\bullet}$, $^{\bullet}OH$, $^{\bullet}O_2^-$ *etc.* The competition between H_2O and OH can also lead to the deactivation of catalyst. Up to now, lots of strategies have been applied to alleviate the adsorption of water on O_3 active sites:

(a) Reduce the hydrophilic functional groups on the catalyst surface and improve the hydrophobic properties. Hydroxyl groups (OH) are widely existed on metal oxides, which can bond with water molecular *via* hydrogen bonding, displaying hydrophilic property. This may partly block the active sites. Furthermore, OH may react with O_3 with the generation of water and inhibit the O_3 decomposition. Liu *et al.* [57] removed surface hydroxyl groups by treating MnO_2 at 300 °C to increase catalyst's O_3 removal efficiency. In addition, the introduction of Ag in MnO_x can also change the catalysts' water resistance characteristic. Deng *et al.* [41] reported that the addition of Ag significantly decreases the interaction between water vapor and the surface of Ag/MnOx catalysts, showing water tolerance property.

(b) Construct a catalyst with suitable pore structures to reduce water adsorption. Li *et al.* [95] fabricated a porous cerium-doped manganese oxides *via* reaction between permanganate, dopamine and Ce^{3+}. The introduction of Ce^{3+} inhibits the growth of MnO_x and gives rise to more macrospores and mesoporous pores. Enlarged pores in Ce–MnO_x can alleviate the deactivation caused by moisture condensation (usually occurs at mesoporous pores less than 20 nm) and therefore contribute to the O_3 decomposition. Moreover, Cao *et al.* [96] synthesized higher porosity MnO_2-based hybrid aerogel using cellulose nanofibers as the framework. The interconnected macrospores facilitate the passage of water molecules. Furthermore, consumed OH on MnO_2 by the coverage of cellulose not only reduce the water adsorption but also avoid the generation of surface-adsorbed H_2O *via* the reaction with O_3.

(c) Adjust the active sites to balance the adsorption of ozone and water molecules. Hong *et al.* [97] modified V_O by introducing manganese vacancy (V_{Mn}) and appropriate amounts of Li^+. The modified structure changes the adsorption energies of O_3, H_2O, and O_2 on MnO_2 surface. Theoretical calculation shows that V_{Mn} and appropriate amounts of Li^+ lower the adsorption energy of O_2 and H_2O molecules dramatically comparing with the unmodified one, but O_3 adsorption is not obviously suppressed. This unique structure shows enhanced water tolerance. In addition, Li *et al.* [53] also calculated O_3, H_2O, and

O_2 adsorption energy at two different V_O sites on the MnO_2 catalysts, *i.e.*, sp^2-V_O and sp^3-V_O. The adsorption energies of O_3 and H_2O both decrease at sp^2-V_O site, which might help to improve the water tolerance. However, the adsorption energy of O_2 increases at sp^2-V_O site, inhibiting the desorption of O_2. Thus, the entire O_3 decomposition process needs to be thoroughly considered especially under humid condition.

(d) Explore water-promoted O_3 decomposition catalysts. Almost all the reported catalysts display decreased O_3 decomposition activity in the presence of moisture because of inevitable competitive-adsorption at active site. Wang *et al.* [33] found that water is involved in O_3 decomposition reaction using Fe-MIL-100 catalyst. The water molecular deprotonates with the formation of hydroxyl at Fe site. The H atom transfer from Fe–OH to O_3 molecule, resulting in the formation of Fe–O species and $HO_3^{\bullet}$ radical. This step is the rate–limiting step with the barrier of 25.5 kcal/mol, which is the highest energy barrier among all pathways. In addition, a water involved O_3 decomposition mechanism was also proposed according the principles of liquid O_3 decomposition [98–100]. Thus, exploring MOF-based catalyst might be a new strategy to overcome the catalyst deactivation caused by moisture.

5. Perspective

The aim of this review is to summarize high-efficient O_3 decomposition catalysts and investigate their potential application in real indoor ventilation system, especially at high relative humidity and short residence time. In order to evaluate the performance of the catalyst more effectively, the O_3 concentration tested is up to tens to thousands of ppm level, which is much higher than that exists in actual indoor environment. Considering the wide use of O_3, catalysts summarized here can also be used for residual O_3 control in the field of industrial catalytic ozonation. Although plenty of O_3 decomposition catalysts have been developed, state-of-the-art catalysts for rapid O_3 decomposition with long-term stability under extreme conditions are still not obtained and their corresponding-intrinsic mechanism is still unclear. Future research efforts are suggested as follows:

(a) Active site regulation. MnO_2 has been widely studied in O_3 catalytic decomposition. At present, it is generally believed that the presence of V_O (unsaturated Mn) significantly improves the catalytic activity of MnO_2. According to the classic O_3 decomposition principle, the desorption of O_2^{2-} on the surface is a rate–limiting step. Future work should be focused on this part by adjusting the coordination structure to reduce the energy barrier of the rate–limiting step.

(b) The function of water. The presence of water can inhibit the O_3 catalytic performance of MnO_2. However, Wang *et al.* [33] found that the water promoted the O_3 catalytic activity over Fe–MOF. Based on the mechanism of liquid–phase O_3 decomposition, Zhu and Wang *et al.* [33,38] proposed a water participated O_3 mechanism, but the free radical reactions involved in this mechanism is still a theoretical hypothesis. Sufficient experimental data is still needed.

(c) New catalysts. MOF material is a new type of catalytic material. At present, only Fe–MOF (MIL–100) was investigated in O_3 decomposition. The central atom in MOF is the active site. By changing the type of organic ligand, the geometric and electronic structure of center metal varies. In addition, the properties of the ligand itself can regulate the hydrophilic and hydrophobic properties of the MOF, which may be more suitable for its practical applications.

(d) Synergistic effect between O_3 and other indoor pollutants. Multiple pollutants coexist in the indoor environment. As an oxidant, O_3 can be used to catalytically oxidize indoor VOCs. This strategy cannot only solve the indoor VOCs pollution, but also eliminate indoor O_3. Furthermore, the oxidation of some VOCs, such as formaldehyde, requires the participation of water, which can alleviate the negative effect of water vapor on most O_3 decomposition catalysts.

Declaration of competing interest

The authors declare that they have no known competing financial interests or personal relationships that could have appeared to influence the work reported in this paper.

Acknowledgments

This project is supported by National Natural Science Foundation of China (Nos. 21707107, 22076150), Fundamental Research Funds for the Central Universities (No. 205208007).

References

[1] B. Dhandapani, S.T. Oyama, Appl. Catal. B: Environ. 11 (1997) 129–166.
[2] T. Batakliev, V. Georgiev, M. Anachkov, S. Rakovsky, Interdiscip. Toxicol. 7 (2014) 47–59.
[3] S. Solomon, R.R. Garcia, F.S. Rowland, D.J. Wuebbles, Nature 321 (1986) 755–758.
[4] D. Mitchell, Proc. Natl. Acad. Sci. 103 (2006) 13567–13568.
[5] M. Shao, Y. Zhang, L. Zeng, et al., J. Environ. Manage. 90 (2009) 512–518.
[6] T. Wang, A. Ding, J. Gao, W.S. Wu, Geophys. Res. Lett. 33 (2006) 1–5.
[7] M. Jerrett, R.T. Burnett, C.A. Pope III, et al., New Engl. J. Med. 360 (2009) 1085–1095.
[8] N.E. Klepeis, W.C. Nelson, W.R. Ott, et al., J. Exposure Sci. Environ. Epidemiol. 11 (2001) 231–252.
[9] C.J. Cros, G.C. Morrison, J.A. Siegel, R.L. Corsi, Indoor Air 22 (2012) 43–53.
[10] C.J. Weschler, A.T. Hodgson, J.D. Wooley, Environ. Sci. Technol. 26 (1992) 2371–2377.
[11] V. Valuntaite, R. Girgždiene, J. Environ. Eng. Landsc. Manage. 15 (2007) 61–67.
[12] C. Weisel, C.J. Weschler, K. Mohan, J. Vallarino, J.D. Spengler, Environ. Sci. Technol. 47 (2013) 4711–4717.
[13] M. Sharma, J.B. Hudson, Am. J. Infect. Control 36 (2008) 559–563.
[14] W.H. Glaze, J.W. Kang, D.H. Chapin, Ozone Sci. Eng. 9 (1987) 335–352.
[15] X.T. Li, J.Z. Ma, H. He, J. Environ. Sci. 94 (2020) 14–31.
[16] M. Namdari, C.S. Lee, F. Haghighat, Build. Environ. 187 (2021) 107370.
[17] C. Subrahmanyam, D.A. Bulushev, L. Kiwi-Minsker, Appl. Catal. B: Environ. 61 (2005) 98–106.
[18] D. Helmig, Atmos. Environ. 31 (1997) 3635–3651.
[19] E.L. Williams, D. Grosjean, Environ. Sci. Technol. 24 (1990) 811–814.
[20] J. Kim, P. Zhang, J. Li, J. Wang, P. Fu, Chem. Eng. J. 252 (2014) 337–345.
[21] J. Patzsch, J.Z. Bloh, Catal. Today 300 (2018) 2–11.
[22] S. Josset, J. Taranto, N. Keller, V. Keller, M.C. Lett, Environ. Sci. Technol. 44 (2010) 2605–2611.
[23] S. Solomon, Rev. Geophys. 37 (1999) 275–316.
[24] B.M. Coldiron, J. Am. Acad. Dermatol. 27 (1992) 653–662.
[25] W. Li, G.V. Gibbs, S.T. Oyama, J. Am. Chem. Soc. 120 (1998) 9041–9046.
[26] W. Li, S.T. Oyama, J. Am. Chem. Soc. 120 (1998) 9047–9052.
[27] H. Valdes, F.J. Ulloa, V.A. Solar, et al., Microporous Mesoporous Mater. 294 (2020)109912.
[28] P.J. Kunkeler, B.J. Zuurdeeg, J.C. van der Waal, et al., J. Catal. 180 (1998) 234–244.
[29] N. Brodu, M.H. Manero, C. Andriantsiferana, J.S. Pic, H. Valdés, Chem. Eng. J. 231 (2013) 281–286.
[30] H. Valdes, S. Alejandro, C.A. Zaror, J. Hazard. Mater. 227 (2012) 34–40.
[31] N. Brodu, M.H. Manero, C. Andriantsiferana, J.S. Pic, H. Valdés, Can. J. Chem. Eng. 96 (2018) 1911–1918.
[32] J.R. Long, O.M. Yaghi, Chem. Soc. Rev. 38 (2009) 1213–1214.
[33] H. Wang, P. Rassu, X. Wang, et al., Angew. Chem. Int. Ed. 57 (2018) 16416–16420.
[34] C. Heisig, W. Zhang, S.T. Oyama, Appl. Catal. B: Environ. 14 (1997) 117–129.
[35] J. Jia, P. Zhang, L. Chen, Appl. Catal. B: Environ. 189 (2016) 210–218.
[36] J. Jia, P. Zhang, L. Chen, Catal. Sci. Technol. 6 (2016) 5841–5847.
[37] S. Liu, J. Ji, Y. Yu, H. Huang, Catal. Sci. Technol. 8 (2018) 4264–4273.
[38] G. Zhu, J. Zhu, W. Jiang, et al., Appl. Catal. B: Environ. 209 (2017) 729–737.
[39] G. Zhu, J. Zhu, W. Li, et al., Environ. Sci. Technol. 52 (2018) 8684–8692.
[40] W. Hong, T. Zhu, Y. Sun, et al., Environ. Sci. Technol. 53 (2019) 13332–13343.
[41] H. Deng, S. Kang, J. Ma, et al., Environ. Sci. Technol. 53 (2019) 10871–10879.
[42] T. Gopi, G. Swetha, S. Chandra Shekar, et al., Catal. Commun. 92 (2017) 51–55.

[43] L. Miao, J. Wang, P. Zhang, Appl. Surf. Sci. 466 (2019) 441–453.
[44] J. Jia, W. Yang, P. Zhang, J. Zhang, Appl. Catal. A 546 (2017) 79–86.
[45] X. Li, J. Ma, L. Yang, et al., Environ. Sci. Technol. 52 (2018) 12685–12696.
[46] J. Ma, C. Wang, H. He, Appl. Catal. B: Environ. 201 (2017) 503–510.
[47] Y. Yang, J. Jia, Y. Liu, P. Zhang, Appl. Catal. A 562 (2018) 132–141.
[48] Y. Yang, P. Zhang, J. Jia, Appl. Surf. Sci. 484 (2019) 45–53.
[49] Y. Yu, J. Ji, K. Li, et al., Catal. Today (2019) 5090–5099.
[50] J. Ma, X. Li, C. Zhang, Q. Ma, H. He, Appl. Catal. B: Environ. 264 (2020) 118498.
[51] J. Jia, P. Zhang, Ozone Sci. Eng. 40 (2018) 21–28.
[52] X. Wang, Y. Li, Mater. Chem. Phys. 82 (2003) 419–422.
[53] X.T. Li, J.Z. Ma, C.B. Zhang, R.D. Zhang, H. He, J. Environ. Sci. 91 (2020) 43–53.
[54] Y. Chen, W. Qu, C. Li, et al., Ind. Eng. Chem. Res. 57 (2018) 12590–12594.
[55] Y. Liu, W. Yang, P. Zhang, J. Zhang, Appl. Surf. Sci. 442 (2018) 640–649.
[56] R. Cao, P. Zhang, Y. Liu, X. Zheng, Appl. Surf. Sci. 495 (2019) 143607.
[57] Y. Liu, P. Zhang, J. Phys. Chem. C 121 (2017) 23488–23497.
[58] Y. Liu, P. Zhang, Appl. Catal. A 530 (2017) 102–110.
[59] Y. Yu, S. Liu, J. Ji, H. Huang, Catal. Sci. Technol. 9 (2019) 5090–5099.
[60] Y. Liu, P. Zhang, J. Zhan, L. Liu, Appl. Surf. Sci. 463 (2019) 374–385.
[61] Z. Lian, J. Ma, H. He, Catal. Commun. 59 (2015) 156–160.
[62] C. Wang, J. Ma, F. Liu, H. He, R. Zhang, J. Phys. Chem. C 119 (2015) 23119–23126.
[63] L. Tao, G. Zhao, P. Chen, et al., ChemCatChem 11 (2019) 1131–1142.
[64] T. Gopi, G. Swetha, S.C. Shekar, et al., Catal. Commun. 92 (2017) 51–55.
[65] L. Yang, J. Ma, X. Li, et al., J. Environ. Sci. 87 (2020) 60–70.
[66] X. Li, J. Ma, C. Zhang, R. Zhang, H. He, J. Environ. Sci. 91 (2020) 43–53.
[67] L. Yang, J. Ma, X. Li, C. Zhang, H. He, Ind. Eng. Chem. Res. 59 (2020) 118–128.
[68] L. Yang, J.Z. Ma, X.T. Li, et al., J. Environ. Sci. 87 (2020) 60–70.
[69] T. Mathew, K. Suzuki, Y. Ikuta, et al., Angew. Chem. 123 (2011) 7519–7522.
[70] S. Gong, W. Li, Z. Xie, et al., New J. Chem. 41 (2017) 4828–4834.
[71] S. Gong, A. Wang, Y. Wang, et al., ACS Appl. Nano Mater. 3 (2020) 597–607.
[72] A.Q. Wang, L. Zhang, M.G. Rahimi, et al., Appl. Catal. B: Environ. 277 (2020) 119223.
[73] R. Radhakrishnan, S.T. Oyama, J.G. Chen, K. Asakura, J. Phys. Chem. B 105 (2001) 4245–4253.
[74] J. Ji, Y. Fang, L. He, H. Huang, Catal. Sci. Technol. 9 (2019) 4036–4046.
[75] S. Gong, J. Chen, X. Wu, N. Han, Y. Chen, Catal. Commun. 106 (2018) 25–29.
[76] S. Gong, Z. Xie, W. Li, et al., Appl. Catal. B: Environ. 241 (2019) 578–587.
[77] S. Gong, X. Wu, J. Zhang, N. Han, Y. Chen, CrystEngComm 20 (2018) 3096–3104.
[78] S.T. Oyama, Catal. Rev. Sci. 42 (2000) 279–322.
[79] Z. Hao, D. Cheng, Y. Guo, Y. Liang, Appl. Catal. B: Environ. 33 (2001) 217–222.
[80] P. Zhang, B. Zhang, R. Shi, Front. Env. Sci. Eng. China 3 (2009) 281–288.
[81] Q. Yu, H. Pan, M. Zhao, et al., J. Hazard. Mater. 172 (2009) 631–634.
[82] L. Yang, J. Ma, X. Li, et al., Catal. Sci. Technol. 10 (2020) 7671–7680.
[83] S. Imamura, M. Ikebata, T. Ito, T. Ogita, Ind. Eng. Chem. Res. 30 (1991) 217–221.
[84] L.G. Tao, Z.Q. Zhang, P.J. Chen, et al., Appl. Surf. Sci. 481 (2019) 802–810.
[85] X.T. Li, J.Z. Ma, H. He, Environ. Sci. Technol. 54 (2020) 11566–11575.
[86] X. Li, J. Ma, C. Zhang, R. Zhang, H. He, J. Environ. Sci. 80 (2019) 159–168.
[87] P. Nikolov, K. Genov, P. Konova, et al., J. Hazard. Mater. 184 (2010) 16–19.
[88] M.C. Wu, N.A. Kelly, Appl. Catal. B 18 (1998) 79–91.
[89] T. Kameya, K. Urano, J. Environ. Eng. 128 (2002) 286–292.
[90] P. Konova, A. Naydenov, P. Nikolov, N. Kumar, J. Porous Mater. 25 (2018) 1301–1308.
[91] H. Metiu, S. Chre'tien, Z. Hu, B. Li, X. Sun, J. Phys. Chem. C 116 (2012) 10439–10450.
[92] Y. Zhang, Inorg. Chem. 21 (1982) 3889–3893.
[93] W. Yang, Y. Zhu, F. You, et al., Appl. Catal. B: Environ. 233 (2018) 184–193.
[94] J. Wang, Y. Dang, A.G. Meguerdichian, et al., Environ. Sci. Technol. Lett. 7 (2020) 48–53.
[95] L.X. Li, P.Y. Zhang, R.R. Cao, Catal. Sci. Technol. 10 (2020) 2254–2267.
[96] R. Cao, L. Li, P. Zhang, J. Harzard. Mater. 407 (2021) 124793.
[97] W. Hong, M.P. Shao, T.L. Zhu, et al., Appl. Catal. B: Environ. 274 (2020) 119088.
[98] L. Zhao, J. Ma, Z. Sun, H. Liu, Appl. Catal. B: Environ. 89 (2009) 326–334.
[99] J. Nawrocki, B. Kasprzyk-Hordern, Appl. Catal. B: Environ. 99 (2010) 27–42.
[100] S. Afzal, X. Quan, J. Zhang, Appl. Catal. B: Environ. 206 (2017) 692–703.